minerals

MDPI

Article

Covalent Protein Immobilization onto Muscovite Mica Surface with a Photocrosslinker

Anastasia A. Valueva, Ivan D. Shumov, Anna L. Kaysheva, Irina A. Ivanova, Vadim S. Ziborov, Yuri D. Ivanov and Tatyana O. Pleshakova *

Institute of Biomedical Chemistry, Pogodinskaya st., 10, 119121 Moscow, Russia; varuevavarueva@gmail.com (A.A.V.); shum230988@mail.ru (I.D.S.); kaysheva1@gmail.com (A.L.K.); i.a.ivanova@bk.ru (I.A.I.); ziborov.vs@yandex.ru (V.S.Z.); yurii.ivanov.nata@gmail.com (Yu.D.I.)

* Correspondence: t.pleshakova1@gmail.com

Received: 31 March 2020; Accepted: 14 May 2020; Published: 20 May 2020

Abstract: Muscovite mica with an amino silane-modified surface is commonly used as a substrate in atomic force microscopy (AFM) studies of biological macromolecules. Herein, the efficiency of two different protein immobilization strategies employing either (N-hydroxysuccinimide ester)-based crosslinker (DSP) or benzophenone-based photoactivatable crosslinker (SuccBB) has been compared using AFM and mass spectrometry analysis. Two proteins with different physicochemical properties—human serum albumin (HSA) and horseradish peroxidase enzyme protein (HRP)—have been used as model objects in the study. In the case of HRP, both crosslinkers exhibited high immobilization efficiency—as opposed to the case with HSA, when sufficient capturing efficiency has only been observed with SuccBB photocrosslinker. The results obtained herein can find their application in commonly employed bioanalytical systems and in the development of novel highly sensitive chip-based diagnostic platforms employing immobilized proteins. The obtained data can also be of interest for other research areas in medicine and biotechnology employing immobilized biomolecules.

Keywords: muscovite mica; atomic force microscopy; crosslinker; protein immobilization

1. Introduction

Surface chemistry plays a crucial role in the development of materials with biological functionality [1] intended for various medical and biotechnological applications, including fabrication of sensor chips for biomarker detection [2–4], development of medical implants [2,5] and enzyme catalysis for wastewater purification [6], food [7–9] and biofuel production [10] etc. In these applications, the necessary biological functionality of a surface is attained by immobilization of various types of biomolecules, such as peptides [5,11], enzymes [10,12,13], antibodies [14–17], aptamers [3,18], glycans [4] etc. That is, the surface to be immobilized with biomolecules must possess chemically active groups capable of binding with the biomolecules of interest under certain conditions that provide retaining of their biological activity.

Regarding biomarker detection applications, surface functionalization with biomolecules is often used in the fabrication of sensor chips used for selective capturing of target marker molecules from the analyzed sample for their subsequent detection on the sensor chip surface [14,16,17]. This principle of capturing target molecules from the volume of the analyzed sample onto the solid surface of a sensor chip was called molecular fishing [14,19]. During the capturing, the chip-immobilized probe molecules selectively bind the target molecules owing to biospecific interaction [2,17,19]. This principle is widely used in various types of biosensor systems [20].

In this field, particular attention is paid to the development of highly sensitive biosensor systems that allow one to detect target marker molecules at low and ultra-low concentrations [21]. The latter can be achieved by using biosensor systems based on molecular detectors—such as the atomic force microscope (AFM), which allows for the detection of biomarkers at the single-molecule level [3,14]. The combination of biomolecular fishing with atomic force microscopy (AFM)-based detection was called AFM-based fishing [14,22]. It has been recently demonstrated that AFM-based fishing allows one to detect protein markers of viral hepatitis C in buffer solutions [23] and in human serum samples [3,16]. In the AFM-based fishing, AFM chips with modified (functional) surface are employed. In the case of biospecific molecular fishing, the active surface of such chips is functionalized with immobilized probe molecules (typically antibodies or aptamers), and target molecules are captured onto the chip surface owing to the biospecific interaction with the chip-immobilized probe molecules. Molecular fishing can also be used for the non-specific capturing of all biomolecules present in the sample. This approach was called chemical fishing [22]. In this latter case, chips with crosslinker-activated surface are employed. This approach is promising for the detection of proteins at ultra-low concentrations [22]. In the present study, the capturing efficiency of crosslinkers, used for the activation of the AFM chip surface, has been considered.

Unprecedented sensitivity of AFM imposes specific requirements to the materials used as substrates for AFM sensor chip (AFM chip) fabrication—namely, their surface roughness. Since AFM provides extremely high (0.1 nm) height resolution of the imaged surface [24], the surface roughness of the sensor chip surface used in AFM-based biosensor system should generally not exceed 1 nm. In addition, the surface of the AFM chip must be free of contaminants and easy to prepare [25]. For these reasons, the list of materials suitable for the fabrication of AFM chips is very limited and includes muscovite mica, silicon, highly oriented pyrolytic graphite (HOPG) and optically flat glass [24,26]. Among these materials, muscovite mica ($KAl_2(OH)_2AlSi_3O_{10}$ [26]) is the most attractive, as its laminate structure allows simple and fast obtaining of clean and, at the same time, atomically smooth surfaces without the need for additional procedures [26]. The unique smoothness of the mica surface makes it excellent material for fabrication of AFM chips intended for visualization of single biological macromolecules—in particular, globular proteins. At the same time, glass can be employed for visualization of elongated biomolecules, such as DNA [25].

It is known that both mica and glass pertain to silicates [26–28]. The surfaces of both mica and glass, however, lack any chemically active groups that could be used for direct covalent attachment of biological probe molecules. Moreover, another requirement to the AFM chip surface consists in that a sufficiently strong interaction between the chip surface and the probe molecules should be provided [25,26]. In some experimental techniques, such as AFM visualization of DNA molecules [29], physical adsorption of biomolecules of interest onto bare mica surface is sufficient. At the same time, immobilization of mica surface with probe molecules for its further use as sensor chip in biomolecular AFM-based fishing requires additional functionalization of this surface to provide chemical groups that can be linked with probe biomolecules-such as proteins (antibodies) or nucleic acids (aptamers). In this respect, treatment with various silanes (silanization) has become a commonly used approach to the functionalization of silicates, including mica and glass surfaces. For this purpose, 3-aminopropyltriethoxysilane (APTES) is employed most frequently [29–35]. The approach employing APTES was proposed by Lyubchenko et al. in one of the pioneer works considering mica silanization [30]. A number of scientific groups have demonstrated excellent suitability of APTES-modified mica for covalent or non-covalent immobilization of DNA [25,29,31–33] and protein [14,16,18,34,35] macromolecules in AFM studies.

While for DNA macromolecules, the interaction with the amino mica surface was shown to be sufficiently strong even in the case of non-covalent adsorption [25,29,31], attachment of protein macromolecules (particularly if they are employed as molecular probes in chip-based AFM analysis) often requires covalent immobilization onto this surface. For this purpose, various additional crosslinking agents, which are capable of reacting with functional groups of both the protein to be immobilized and the chip surface, are commonly employed [36]. Below, we will consider the protein

immobilization approaches onto amino silane-modified surfaces of AFM substrates in some more detail.

For this purpose, one can use either bifunctional crosslinkers or two-component systems. Regarding the latter, a system containing a mixture of N-hydroxysuccinimide, NHS (or its better soluble analogue N-hydroxysulfosuccinimide sodium salt, sulfo-NHS) with 1-ethyl-3-(3-dimethylaminopropyl) carbodiimide, EDC (commonly known as NHS/EDC chemistry) is widely employed. An advantage of using NHS/EDC is its universality, as with this chemistry proteins can be immobilized onto a surface with either carboxylic [37,38] or primary amine [15,39] functionality, depending on immobilization conditions. Another advantage of using this chemistry is that preliminary activation of the substrate surface is not mandatory. That is, a mixture of NHS/EDC solution with macromolecules to be immobilized can be directly applied onto the substrate surface. However, since NHS/EDC chemistry activates carboxylic groups of proteins directly in solution, this often leads to an undesired formation of large covalently cross-linked aggregates of proteins, which are immobilized onto the substrate surface instead of single protein molecules. If the substrate surface bears carboxylic functionality, this issue can be simply avoided by preliminary activation of the surface with NHS/EDC [38]. Amino silane-modified mica is not the case. This is a serious disadvantage of using NHS/EDC system for immobilization of proteins intended for use as molecular probes in chip-based analysis, particularly so highly sensitive one as AFM.

Bifunctional crosslinkers for protein immobilization can be divided into several types depending on their chemical type. Glutaraldehyde is one of such crosslinkers, which is widely used for protein immobilization onto sensor surfaces bearing primary amine groups [40]. However, action of glutaraldehyde on amino silane surface leads to a significant increase in its roughness, as was clearly demonstrated by AFM in the study by Carvalho et al. [41]. Moreover, it is to be noted that upon using glutaraldehyde, protein attachment to an amino-functionalized surface occurs via formation of Schiff bases. The Schiff bases are known to be unstable under acidic conditions, what leads to their destruction and corresponding loss of the biological functionality of the surface [40]. The latter issue can be avoided by using borohydrides as reducing agents [40,42]. Nevertheless, it should be emphasized that borohydride may affect the functional activity of the immobilized protein due to the undesired cleavage of disulfide bonds within the protein macromolecules [42]. This is particularly important in the case when enzymes are to be immobilized [43,44].

Another type of bifunctional crosslinkers is represented by N-hydroxysuccinimide esters. They are capable of reacting with primary amine groups, and can accordingly be well employed for covalent attachment of biomacromolecules with available primary amine groups onto amino silane surfaces [36]. Dithiobis(succinimidyl carbonate) (DSC), dithiobis(succinimidyl propionate) (DSP), and dithiobis(sulfosuccinimidyl propionate) (DTSSP) are commonly used N-hydroxysuccinimide crosslinkers [42]. In this way, we previously demonstrated successful use of DSC for covalent capturing of horseradish peroxidase (HRP) protein from 10^{-17} M aqueous solution onto APTES-modified mica. Application of chemical AFM-based fishing allowed us to detect HRP in solution at ultra-low concentration [22].

Nevertheless, upon using (N-hydroxysuccinimide ester)-based crosslinkers, a competing reaction of hydrolysis of active succinimide groups occurs [36], what causes their degradation and corresponding decrease in surface density of immobilized probe molecules on the chip surface. Since the latter is a critical point in chip-based AFM analysis, susceptibility of succinimide groups to hydrolysis is a disadvantage of using (N-hydroxysuccinimide ester)-based crosslinkers.

Another type of crosslinkers is photocrosslinkers. These compounds bear a functional group that can be activated by irradiation with light of a certain wavelength, and, in the activated state, is capable to covalently bind proteins.

One type of photocrosslinkers is represented by aryl azides [36]. It is interesting to note that a photocrosslinker with aryl azide functionality was employed in one of the very first techniques of protein immobilization onto an amino silane surface; this technique was proposed in 1993 by Karrasch et al. [45]. These authors have developed a protocol of in situ treatment of APTES-modified glass surface with a photoactivatable N-5-azido-2-nitrobenzoyloxysuccinimide crosslinker. After

such a treatment, photoreactive azide functional groups were exposed on the glass surface. Despite the latter became hydrophobic after the treatment, the authors demonstrated successive immobilization of proteins for their subsequent study by AFM. The main disadvantage of using crosslinkers with aryl azide functionality is the irreversible photoactivation of azide groups, while the lifetime of azide group in activated state (nitrene) is short (of the order of 10^{-13} s [46]). That is, if an activated azide group does not interact with a macromolecule of protein to be immobilized, its functionality is lost irreversibly. Another disadvantage of using aryl azides is that their maximum activation wavelength is often less than 300 nm, which can result in damage of the biomolecules to be immobilized [47]. To minimize damage to the biomolecules, light bandpass filters should be employed.

Benzophenone-type photocrosslinkers are devoid of the disadvantage regarding the irreversible loss of functionality typical for aryl azides. 4-benzoylbenzoic acid N-succinimidyl ester (SuccBB) is a typical representative of this type of photocrosslinkers. This crosslinker contains benzophenone residue, which readily reacts with proteins upon irradiation [47,48]. Moreover, activated benzophenone group does not degrade irreversibly, if it is not involved in bond formation; unreacted benzophenone can be photolyzed again to form a covalent bond with a protein [42,49]. The photoactive groups are excited at a wavelength of 350 to 370 nm. This is another significant advantage of benzophenone-type photocrosslinkers, since irradiation at this wavelength does not damage biological macromolecules [47]. Moreover, another significant advantage of benzophenone-type crosslinkers over aryl azides is the lifetime of their active group in excited state, which can reach 80 to 120 μs, what is 7 orders of magnitude longer than that of nitrene group in case of aryl azides [48]. Application of benzophenones for mapping the conformations of flexible chains in solution, micelles, and membranes [50], and for mapping nucleotide binding sites in ATPases [51] was demonstrated. In [52], Prestwich et al. showed that benzophenone-type crosslinkers have higher crosslinking yields in comparison with aryl azides. Tsai et al. [53] demonstrated that use of APTES-modified glass chips, treated with SuccBB and BSA, allows for covalent attachment of target proteins without breaking their structural conformation. In this way, an immunoassay can be performed on the substrate surface. By AFM, Wu et al. [54] demonstrated that the immobilization efficiency of bovine serum albumin onto APTES-modified quartz is much higher upon using benzophenone crosslinker—in comparison with that upon using maleic anhydride.

Herein, AFM has been employed to perform a comparative study of the protein binding efficiency of two different types of crosslinkers—succinimide crosslinker (DSP) and benzophenone photoactivatable crosslinker (SuccBB). In our experiments, we have studied the efficiency of protein capturing onto APTES-modified muscovite mica surface, activated with either DSP or SuccBB crosslinkers, from low-concentration (nanomolar, 10^{-9} M) aqueous solutions of two model proteins with different physicochemical properties: horseradish peroxidase (HRP) and human serum albumin (HSA). The nanomolar protein concentration has been selected, since this concentration range is of interest for analytical proteomics applications—such as highly sensitive AFM-based protein fishing [22].

Horseradish peroxidase (HRP) represents a heme-containing enzyme with a molecular weight of 40 to 44 kDa [55,56]; HRP macromolecule contains 18% to 27% of carbohydrate chains, which stabilize its structure [56–58]. Despite several isoforms of this enzyme are known, C-isoforms are the most abundant ones. The isoelectric points (*pI*) of C1 and C2 isoforms are 9.4 and 9.68, respectively [59].

Human serum albumin (HSA) is a globular protein with a molecular weight of ~66.4 kDa [60] and isoelectric point *pI* = 4.7 to 5.1 (depending on the amount of bound fatty acids) [61].

In our previous study [22], with the example of HRP model protein, the preliminary chemical activation of the AFM chip surface was demonstrated to be an efficient way to capture the protein from its solution with ultra-low (subpicomolar) concentration. Herein, two different types of crosslinkers have been employed for capturing the model proteins from their low-concentration (nanomolar) solutions onto the crosslinker-activated surface of the AFM substrate. At that, we have intentionally selected two proteins—HRP and HSA—whose properties are quite different. The sizes

of HRP and HSA are comparable, and this has been expected to help us to clearly demonstrate how the difference in their properties influences the capturing efficiency.

The elaboration of efficient protein immobilization strategies is a crucial step in the development of novel biosensor systems employing a combination of chip-based analysis (involving chip-immobilized probe molecules) with ultra-sensitive molecular detectors. Such highly sensitive chip-based biosensor systems are in great demand for use in early diagnostics of diseases in human. The results obtained herein can also find their application in other research areas in medicine and biotechnology employing immobilized biomolecules.

2. Materials and Methods

2.1. Proteins

Peroxidase from horseradish (HRP) was purchased from Sigma (Cat.# 6782; St. Louis, MO, USA). Human serum albumin (HSA Standard) was purchased from Agilent (Santa Clara, CA, USA). Porcine trypsin was from Promega Corp. (Cat.# V5111, Madison, WI, USA). Promega Sequencing Grade Modified Trypsin is a porcine trypsin modified by reductive methylation, rendering it resistant to proteolytic digestion.

2.2. Chemicals

Dithiobis(succinimidyl propionate) was purchased from Pierce (Waltham, MA, USA); 4-benzoylbenzoic acid (N-succinimidyl ester) (SuccBB) was purchased from Invitrogen (Carlsbad, CA, USA); 3-aminopropyltriethoxysilane (APTES) was purchased from Acros Organics (Fair Lawn, NJ, USA). Dimethyl sulfoxide (DMSO) was purchased from Sigma (St. Louis, MO, USA). Emulgen 913 was purchased from Kao Atlas (Osaka, Japan). Acetonitrile was purchased from Merck (Darmstadt, Germany). Ethanol (96%, *v*/*v*) was purchased from Reakhim (Moscow, Russia). Peptide calibration standards, 3-fluoroacetic acid and ammonium bicarbonate were from Sigma (St. Louis, MO, USA); α-cyano-4-hydroxycinnamic acid and was from Acros Organics (Fair Lawn, NJ, USA).

Ultrapure deionized water used throughout the study was obtained with a Millipore Simplicity UV deionizer (Millipore, Molsheim, France).

2.3. Modification and Activation of AFM Substrate Surface

Muscovite mica sheets (SPI, West Chester, PA, USA) cut into 7 mm × 15 mm pieces were used as a material for AFM substrates. The surface modification of the muscovite mica substrates with APTES was carried out by the vapour deposition method developed by Yamada et al. [62]. Figure 1 schematically illustrates the main steps of activation of amino mica substrate surface with either DSP or SuccBB crosslinker and subsequent immobilization of a protein under study (HRP or HSA).

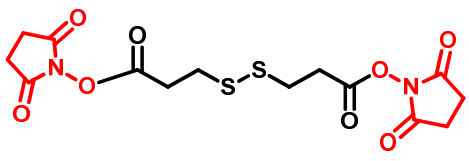

(**A**) DSP crosslinker

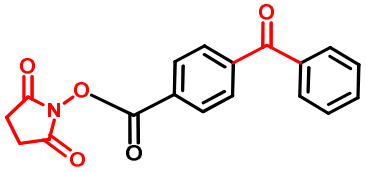

(**B**) SuccBB crosslinker

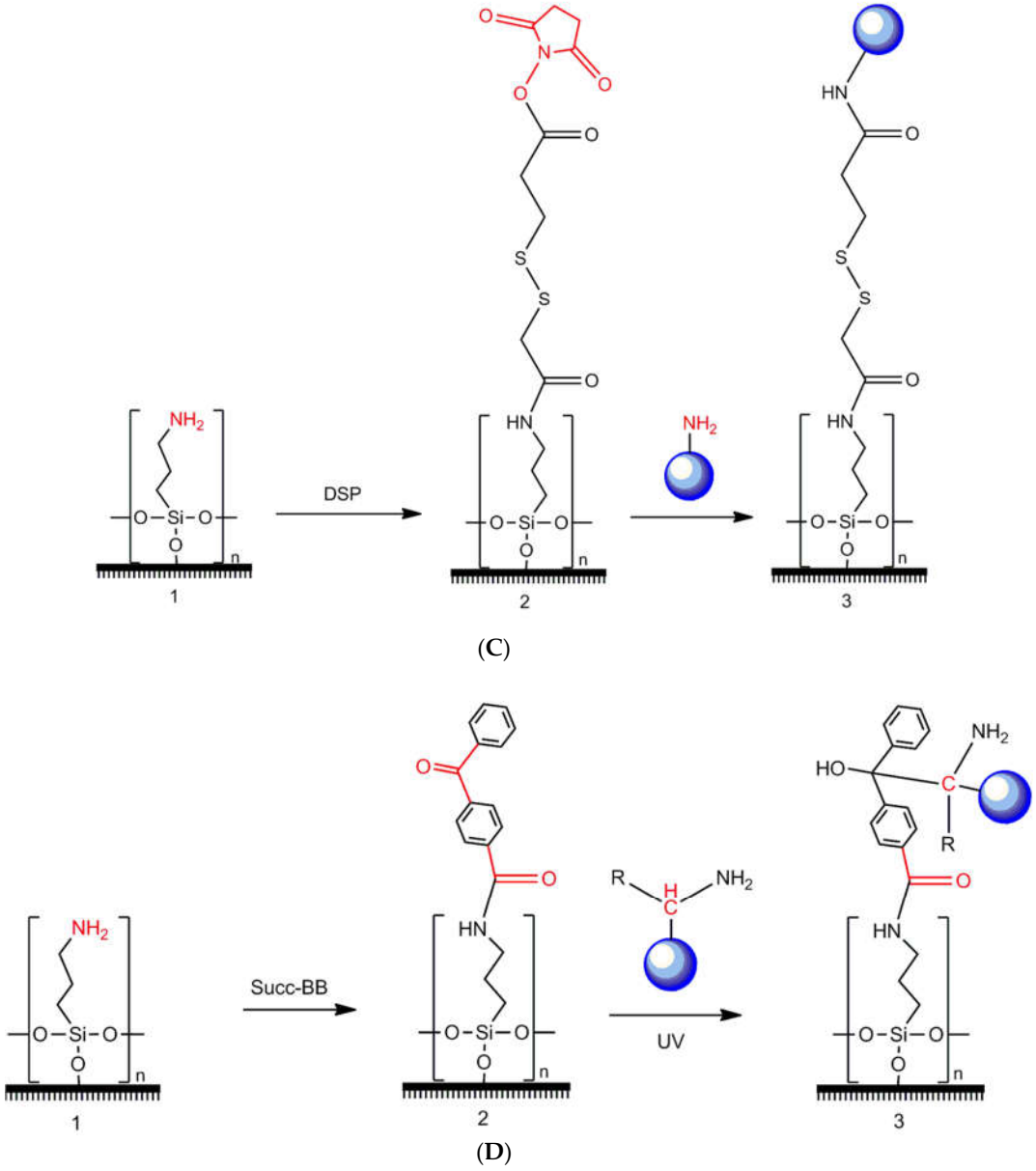

Figure 1. Schematic representation of activation of amino mica substrate surface with a crosslinker and subsequent immobilization of a protein under study onto the activated surface. Panels (**A**) and (**B**) show structural formulae of DSP and SuccBB, respectively. Panels (**C**) and (**D**) schematically illustrate modification of the substrate surface with DSP and SuccBB, respectively, and subsequent immobilization of protein onto the activated surface. 1—amino mica surface; 2—crosslinker-activated substrate surface; 3—substrate surface with immobilized protein. Functional groups of compounds directly involved into chemical reactions on the surface are shown in red. Blue circles indicate protein macromolecules: horseradish peroxidase (HRP) or human serum albumin (HSA).

In case of activation of the substrate surface with DSP crosslinker (Figure 1A), 1.2 mM solution of DSP in DMSO:EtOH (1:1) was mixed with Dulbecco's modified phosphate buffered saline (PBS-D; 50 mM, pH 7.4) in 1:1 ratio (*v*/*v*), and then immediately dispensed onto the AFM substrate surface. After a 10 min incubation of the crosslinker solution on the substrate surface, the substrate was washed in 1 mL of 50% (*v*/*v*) ethanol for 10 min and dried in nitrogen stream. The so-prepared AFM substrates were immediately used for protein immobilization.

In case of SuccBB crosslinker (Figure 1B), 3.1 mM solution of SuccBB in DMSO was dispensed onto the AFM substrate surface and incubated thereon for 30 min at room temperature. After the incubation, the AFM substrate was washed once in 1 mL of DMSO:EtOH (1:1) at 50 °C for 30 min, and then twice in 1 mL of 50% (*v*/*v*) ethanol for 30 min. After washing, the AFM substrate was dried in nitrogen stream and was ready for protein immobilization.

2.4. Covalent Immobilization of Protein

In case of DSP-activated surface, the AFM substrate was incubated in 1 mL of 10^{-9} M aqueous solution of either HRP or HSA in a rotating cuvette at 25 °C and 600 rpm for 60 min (Figure 1C).

In case of SuccBB-activated surface, the AFM substrate was incubated in 1 mL of 10^{-9} M aqueous solution of either HRP or HSA in a rotating cuvette upon UV irradiation at 25 °C and 600 rpm for 60 min (Figure 1D). The irradiation was carried out with an array of eighteen U330A4V138Z2 UV LEDs (Bytech Electronics CO., Zhongshan, China), and the UV light parameters were as follows: wavelength 360 to 370 nm, radiation power ~75 mW. The distance between the cuvette and the UV light source was 2 cm.

AFM substrates, activated with either DSP or SuccBB and immobilized with protein as described above, were then washed once in 1 mL of 0.01% aqueous solution of Emulgen 913 at 37 °C for 30 min, then twice in 1 mL of ultrapure water at 37 °C for 30 min, and dried in air.

Control experiments were carried out as described above, but with following differences:

(1) To estimate the amount of non-protein particles adsorbed onto the surface, crosslinker-activated AFM substrates were incubated in protein-free solution (Control 1);

(2) To estimate the amount of non-specifically (i.e., non-covalently) adsorbed protein macromolecules, the AFM substrates, whose surface was not activated with a crosslinker, were incubated in either HRP or HSA solutions (Control 2).

2.5. AFM Scanning

AFM scanning was performed with a Dimension FastScan Bio atomic force microscope (which pertains to the equipment of "Human Proteome" Core Facility of the Institute of Biomedical Chemistry, Moscow, Russia, supported by Ministry of Education and Science of Russian Federation, agreement 14.621.21.0017, unique project ID RFMEFI62117X0017) (Bruker, Billerica, MA, USA) in ScanAssist mode using AppNano cantilevers (AppNano, Mountain View, CA, USA). The scan size was 5 μm × 5 μm, the number of scans was no less than $n = 16$, and the total scanned area was no less than $S_{scan} = 400$ μm^2. The results of the measurements are presented in the form of 2D images. In a 2D mode, the height of visualized objects is indicated with a single colour of variable intensity. Height, expressed in nanometer units, is the measured parameter of the visualized objects. The height measurement accuracy was 0.1 nm.

2.6. Processing of AFM Images

Processing of AFM images was performed using an AFM data processing software developed in Institute of Biomedical Chemistry (Rospatent registration No. 2010613458) as described elsewhere [3]. The height of AFM-registered objects was the main criterion of determination of their size [24,63].

2.7. Preparation of the AFM Substrate for Mass Spectrometry Measurements

Previously, in our studies considering the protein detection at ultra-low (10^{-9} M and lower) concentrations in solutions and in biological fluid samples (serum), we have selected optimal conditions for the hydrolytic digestion of proteins on the surface of an AFM chip [18,64,65].

In both working and control experiments, the trypsinolysis of protein objects was performed directly on the surface of AFM substrates, onto which 70 μL of incubation solution including 1% acetonitrile (0.7 μL), 0.1 μM of modified trypsin (1.75 μL) in 100 mM bicarbonate buffer (pH 7.4) were added. This was followed by desalination of the so-obtained mixture containing peptide fragments

using ZipTip C18 tips (Millipore, Temecula, CA, USA) according to the manufacturer's protocol supplied to the time-of-flight (TOF) mass-spectrometer for measurements [64,66].

2.8. Mass Spectrometry Measurements

2.8.1. MALDI-TOF Measurements

Protein identification was carried out using Autoflex III TOF mass-spectrometer (Bruker Daltonik GmbH, Bremen, Germany) equipped with nitrogen laser with an emission wavelength of 337 nm. Calibration of the mass spectrometer was performed using a peptide calibration standard for positive ions in the reflector mode with a voltage of 3.5 to 4.0 kV. The recorded mass spectrum was 750 to 3000 m/z with a pulse delay time of 200 ns. The peptide calibration standard included the following peptides (the corresponding monoisotolic single-protonated ionic mass of each peptide is shown in brackets): bradykinin (757.3992 Da), angiotensin II (1046.5420 Da), angiotensin I (1296.6853 Da), R peptide (1347.7361 Da), bombesin (1619.8230 Da), renin (1758.9326 Da), ACTH fragment 1–17 (2093.0868 Da), ACTH fragment 18–39 (2465.1990 Da), and somatostatin (3147.4714 Da). The spectrum analysis excluded the peaks of matrix and trypsin autolysis. The mass spectrum was accumulated in auto mode until the sample spread onto the target was exhausted (typically 50,000 shots). To obtain mass spectra of the samples, the hydrolyzed mixture was mixed with excessive matrix (HCCA in 50% acetonitrile solution in 0.7% TFA) at a ratio ranging from 1:1000 to 1:10,000, and the resulting mixture was spread onto a MTP AnchorChip 384 target [64,66].

The mass spectra were processed with flexAnalysis 2.0 software (Bruker Daltonik GmbH, Bremen, Germany). The protein identification was performed with Mascot proteomic search engine (http://www.matrixscience.com) using the protein sequencing data library SwissProt_2012. The following search options were selected: taxonomic group was human or eukaryotes; two missed hydrolysis sites; the acceptable measurement accuracy of monoisotopic masses was less than 150 ppm; methionine oxidation was indicated as a possible modification [64,66].

2.8.2. Selected Reaction Monitoring MS (SRM-MS) Measurements

The SRM experiments were performed with an Agilent 6495 Triple Quadrupole LC/MS system (Agilent, Santa Clara, CA, USA) equipped with a nano-electrospray ionization source. Samples with a volume of 1 μL were injected into the nano-chromatographic column of a Zorbax 40 chip system. The column dimensions were 75 μm × 43 mm × 5 μm (NL SB-C18 column). The separation of peptides was conducted using solution A (0.1% formic acid in deionized water) and solution B (0.1% formic acid in 90:10 acetonitrile: deionized water, *v*/*v*). Elution of peptides from the chromatographic column was carried out in a gradient of solution B from 0% to 80% for 80 min according to the following scheme: 0 min, 5% solution B; 45 min, 45% solution B; 60 min, 100% solution B; and 75 min, 5% solution B.

The flowrate through the capillary pump was constant (3 μL/min), and the flowrate through the nanopump was 0.3 μL/min. The sample separation was conducted on a nanoLC column (Zorbax RRHD, 50 mm × 0.2 mm, 60 μm particles, 100 Å pore size; Agilent, Santa Clara, CA, USA). The ionization voltage was 19 kV; Q1 and Q3 resolution was 0.7.

Each concentration point was measured in three technical replicates. The control was performed before each measurement. The cut-off line between the signal and the noise was taken as 30 absolute units.

3. Results

On the first step of the study, control experiments have been performed. In the control experiments, the AFM substrate, whose surface was preliminarily activated with either DSP crosslinker or SuccBB photocrosslinker, was incubated in protein-free ultrapure water (Control 1). Figure 2 displays typical AFM images obtained in these control experiments. As one can see from these images, the number of objects with >1 nm height, visualized after the incubation of either DSP-

activated of SuccBB-activated substrate in protein-free water, does not exceed the noise level (which makes up ~30 objects per 25 μm² [22]).

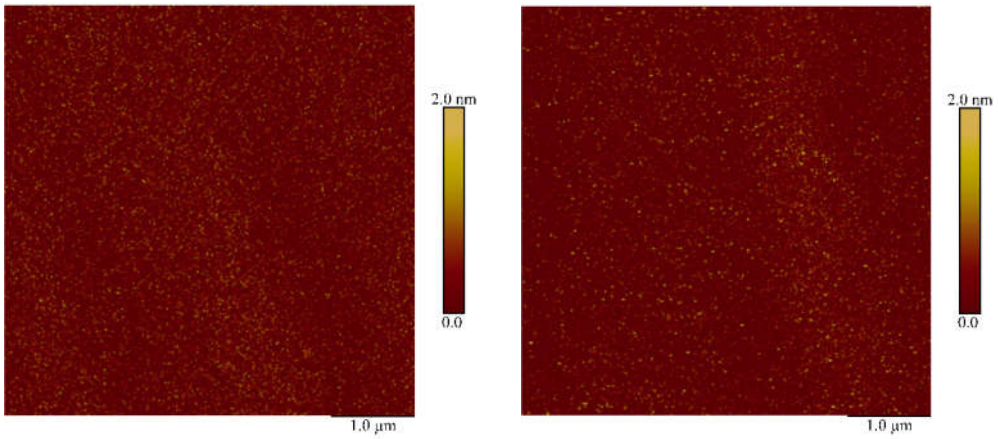

(**A**) (**B**)

Figure 2. Typical atomic force microscopy (AFM) images obtained after incubation of DSP-activated (**A**) and SuccBB-activated (**B**) APTES-modified mica in water (Control 1).

3.1. Immobilization of HRP

Figure 3 displays typical AFM images obtained in working experiments on the immobilization of HRP onto DSP-activated amino mica surface (Figure 3A), and in control experiment with non-activated amino mica (Figure 3B).

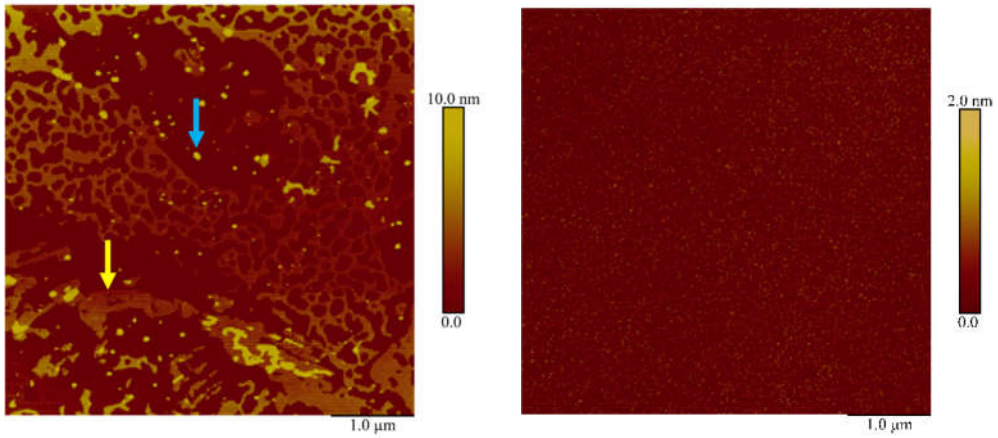

(**A**) (**B**)

Figure 3. Typical AFM images obtained after incubation of DSP-activated (**A**) and non-activated (**B**) APTES-modified mica in 10^{-9} M HRP solution. Yellow arrow indicates the fragment of a layer-like structure, and blue arrow indicates aggregate structures, which have been attributed to layers of immobilized HRP molecules, since no such objects were observed in control experiments.

As seen from Figure 3A, both layer-like and extended aggregate structures are visualized after immobilization of HRP onto the DSP-activated substrate surface. Extended objects of significant lateral sizes, whose height exceeds 1 nm, have been attributed to layer-like structures. In Figure 3A, an example of such layer-like structure is indicated with yellow arrow. The height of layer-like structures makes up 1.6 to 5 nm. The objects of compact shape with heights greater than 5 nm have been attributed to aggregate structures. The lateral sizes of such aggregate structures were small, and their heights reached ~10 nm. An example of such structure is indicated by blue arrow in Figure 3A.

At the same time, in the control experiment with non-activated substrate, neither layer-like nor extended aggregate structures were observed on the substrate surface (Figure 3B; Control 2), and the number of visualized objects with height >1 nm amounted to ~207 particles per 400 μm^2—what is comparable with the noise level determined for AFM-based fishing in [22]. Accordingly, layer-like and extended aggregate structures, visualized in working experiments, can be attributed to HRP oligomers covalently immobilized on the DSP-activated surface. By dynamic light scattering, Ignatenko et al. demonstrated that native HRP can form dimeric and higher-order oligomeric aggregates, whose size in solution is typically ~13 nm, but can reach ~170 nm [67]. In this connection, it is the HRP oligomers that are visualized by AFM as ~10-nm-high compact aggregate structures. The formation of extended layer-like structures on the AFM substrate surface can be explained by the influence of protein-surface interactions. The layer-like structures are apparently formed by predominantly dimeric aggregates of HRP.

To unambiguously identify the proteins, captured onto the AFM substrate surface, one can use various methods (mass spectrometry, immunoassay-based ones, etc.). In our present study, mass spectrometry has been employed.

MS analysis was performed for all samples obtained after AFM experiments with HRP. HRP protein was revealed by MALDI-MS neither in working nor in control experiments. The decrease of MALDI-MS analysis sensitivity in the case of HRP identification (as compared with HSA identification, see Section 3.2 below) is probably explained by the following factor. In theory, there are several (about 30) tryptic fragments for HRP, while for HSA there are more than 90 fragments [68]. Thus, it was necessary to employ a more sensitive triple quadrupole type mass spectrometer. This MS device allowed us to identify HRP fragments in the samples obtained after AFM experiments with capturing of HRP from 10^{-9} M solution.

Selected reaction monitoring (SRM) MS approach allowed us to reliably identify HRP fragments on the surface of DSP-activated amino mica incubated in 10^{-9} M HRP solution (Table 1).

Table 1. The list of transitions for selected reaction monitoring (SRM) analysis, obtained in experiments with DSP-activated (working experiment) and non-activated (control experiment) AFM substrate surface incubated in 10^{-9} M HRP solution.

Experiment	Peptide Sequence	Parent Ion (*m*/*z*)	Fragment Ion (*m*/*z*)	RT*	Height	Width	Area	CE*
working	YYVNLEEQK	593.293	760.384	8.97	570	0.07	2601	23.3
	TPTIFDNK	468.245	737.383	8.60	776	0.073	3833	19
	DTIVNELR	480.261	630.357	9.57	7212	0.068	32205	16.5
	DAFGNANSAR	511.736	689.333	4.93	2159	0.061	8683	22.1
control	YYVNLEEQK	593.293	859.452	0	0	0	0	23.3
	TPTIFDNK	468.245	737.383	0	0	0	0	19
	DTIVNELR	480.261	630.357	0	0	0	0	16.5
	DAFGNANSAR	511.736	689.333	0	0	0	0	22.1

CE*, collision energy; RT*, retention time.

The obtained SRM MS data indicated that 10^{-9} M concentration was sufficient for the identification of the target objects (HRP molecules) captured onto the DSP-activated substrate surface. MS analysis of the samples obtained in control experiments indicated the absence of the target protein on the AFM substrate surface.

Similar measurements were performed for the studied proteins using SuccBB photocrosslinker. Figure 4 displays typical AFM images obtained in working experiments on immobilization of HRP onto SuccBB-activated amino mica surface, and in control experiment with non-activated amino mica. Both working and control experiments were carried out upon UV irradiation at a wavelength of 360 to 370 nm.

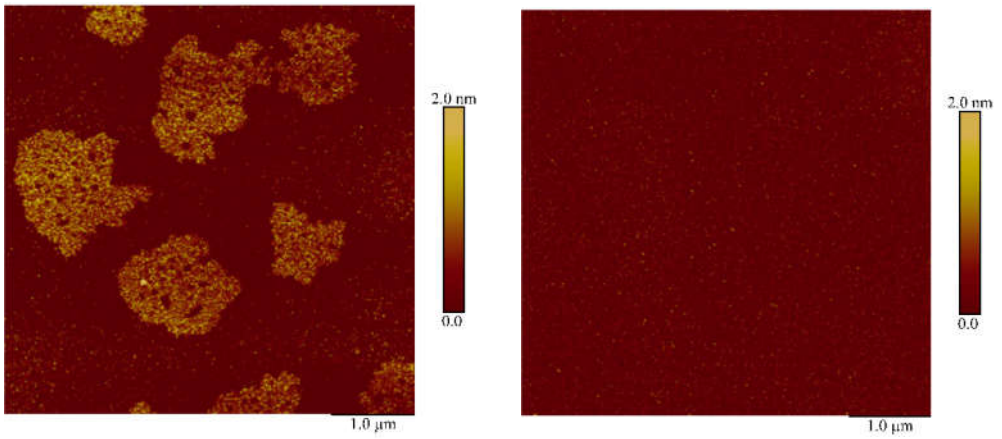

(**A**) (**B**)

Figure 4. Typical AFM images obtained after incubation of SuccBB -activated (**A**) and non-activated (**B**) APTES-modified mica in 10^{-9} M HRP solution upon UV irradiation.

As seen from Figure 4A, a major amount of the visualized objects represents extended structures with a height of ~1.4 ± 0.2 nm. At the same time, such structures were not observed in control experiment with non-activated substrate (Figure 4B; Control 2), while the number of visualized objects made up ~312 particles per 400 μm^2—which is comparable with the noise level [22]. Accordingly, extended structures visualized in working experiments can be attributed to HRP aggregates, which are covalently immobilized on the SuccBB-activated surface.

To confirm the presence of HRP on the substrate surface, SRM-MS measurements were performed analogously to the above-described case with DSP-activated substrates. This approach allowed us to reliably identify HRP fragments on the surface of SuccBB-activated amino mica incubated in 10^{-9} M HRP solution (Table 2).

Table 2. The list of transitions for SRM analysis, obtained in experiments with SuccBB-activated (working experiment) and non-activated (control experiment) AFM substrate surface incubated in 10^{-9} M HRP solution.

Experiment	Peptide Sequence	Parent Ion (*m*/*z*)	Fragment Ion (*m*/*z*)	RT*	Width	Area	CE*
working	YYVNLEEQK	593.293	760.384	8.69	0.071	140	23.3
	TPTIFDNK	468.245	737.383	8.339	0.071	230	19
	DTIVNELR	480.261	630.357	9.364	0.079	3652	16.5
	DAFGNANSAR	511.736	689.333	4.704	0.072	2308	22.1
control	YYVNLEEQK	593.293	859.452	0	0	0	23.3
	TPTIFDNK	468.245	737.383	8.355	0.011	3	19
	DTIVNELR	480.261	630.357	9.34	0.088	17	16.5
	DAFGNANSAR	511.736	689.333	0	0	0	22.1

CE*, collision energy; RT*, retention time.

The obtained SRM MS data indicated that 10^{-9} M concentration was sufficient for the identification of the target objects (HRP molecules) captured onto the SuccBB-activated substrate surface. MS analysis of the samples obtained in control experiments indicated the absence of the target protein on the AFM substrate surface.

As seen from Table 2, in the control experiments, mass spectrometric signals, whose *m*/*z* characteristics and retention times correspond to those of the target peptides, were registered for two of four peptides. However, their intensities, chromatographic peak areas and chromatographic peak shapes (data not shown) are insufficient for their unambiguous identification and are at the level of technical noise. Such insignificant background signal can be caused by possible presence of impurities in the studied protein preparations and components of application and elution buffers in chromatographic tubing fittings.

3.2. Immobilization of HSA

Figure 5 displays typical AFM images obtained in working experiments on immobilization of HSA onto DSP-activated amino mica surface. As seen from this Figure 5A, neither compact objects nor layer-like or aggregate structures are virtually observed on the visualized surface—as opposed to the case with HRP protein. The image obtained in control experiment with non-activated substrate has similar appearance (Figure 5B; Control 2).

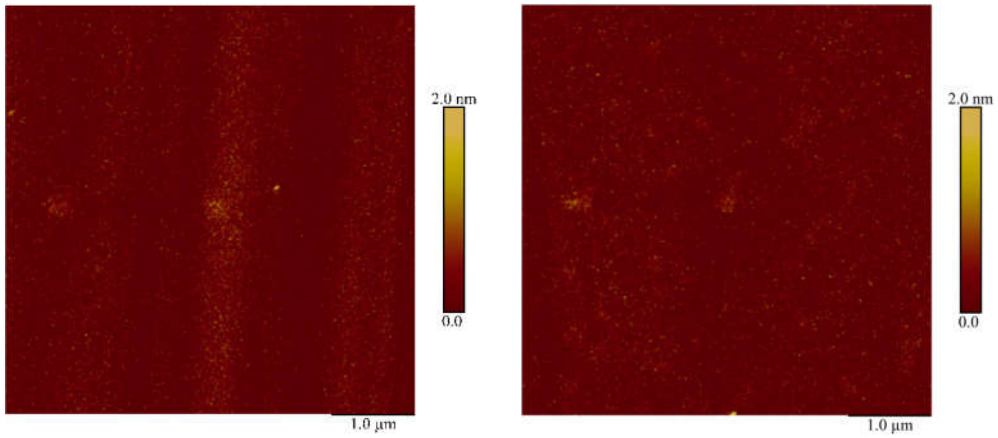

(**A**) (**B**)

Figure 5. Typical AFM images obtained after incubation of DSP-activated (**A**) and non-activated (**B**) APTES-modified mica in 10^{-9} M HSA solution.

Upon analysis of the obtained AFM images, the amount of the registered objects did not exceed that corresponding to the noise level of 500 objects per 400 μm^2 [22]. This indicates immobilization inefficiency under the experimental conditions.

MS analysis of the samples obtained in the control experiments also confirmed the absence of immobilized target protein on the AFM substrate surface. The results of the MS analysis did not allow us to identify the target HSA protein on the surface of DSP-activated amino mica (data not shown).

Figure 6 displays typical AFM images obtained in working experiments on immobilization of HSA onto SuccBB-activated amino mica surface, and in control experiments with non-activated substrates, upon UV irradiation.

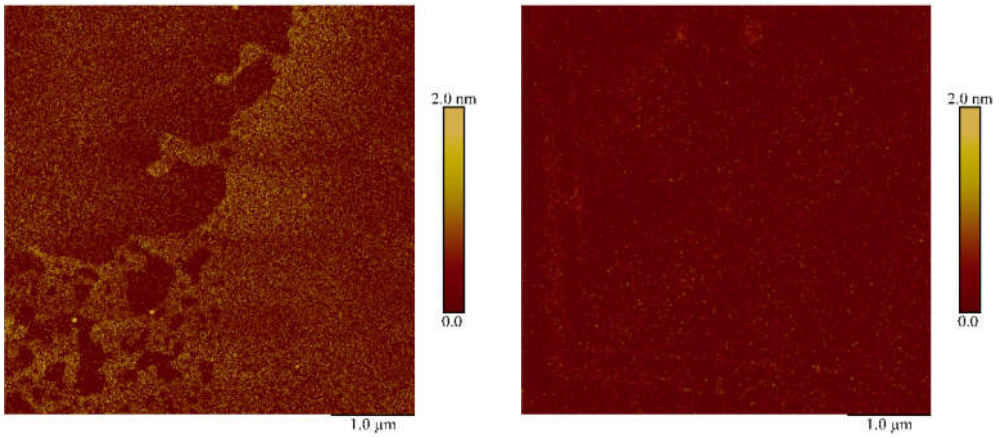

(**A**) (**B**)

Figure 6. Typical AFM images obtained after incubation of SuccBB-activated (**A**) and non-activated (**B**) APTES-modified mica in 10^{-9} M HSA solution upon UV irradiation.

As seen from Figure 6, an 1.4 nm-thick layer is visualized on the surface of SuccBB-activated AFM substrate after its incubation in HSA solution (Figure 6A). Since no such layer was visualized in control experiments (Figure 6B; Control 2), its formation in working experiments can be attributed to immobilized HSA. Our data is in agreement with that obtained earlier by Kowalczyk et al. [69]. Kowalczyk et al. [69] reported the AFM-measured thickness of covalently immobilized HSA molecules to be 3 ± 0.2 nm.

MS analysis of the samples obtained in control experiments showed that the target protein is not adsorbed onto the AFM surface. Thus, the peptide region of the obtained spectra contained no signals of HSA peptide fragments, while the peaks of trypsin autolysis were registered.

Next, the results of MS analysis have indicated that the target HSA protein could only be identified on the substrates activated with SuccBB crosslinker. Peptide fragments of HSA were found in all MS spectra related to these experimental series (Figure 7). Figure 7 displays representative MALDI spectrum of the hydrolyzed objects captured onto the AFM substrate surface from 10^{-9} M HSA solution. Analysis of these spectra allowed reliable identification of HSA protein by 11 peptides with an analysis reliability of 95%.

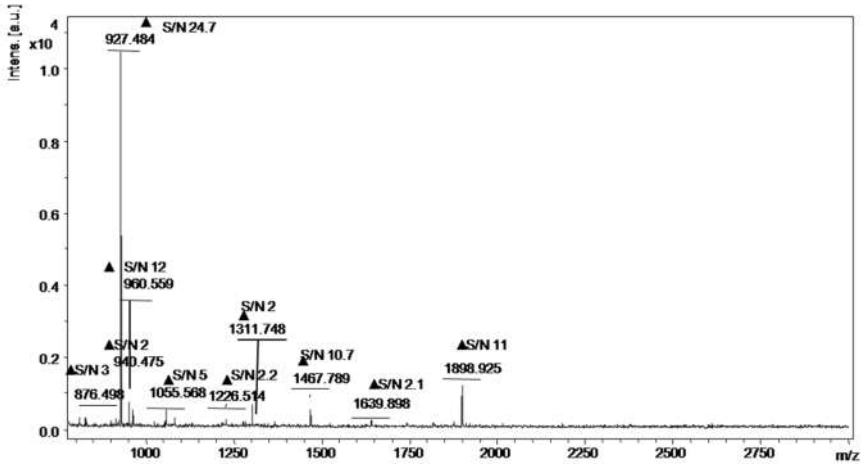

(**A**)

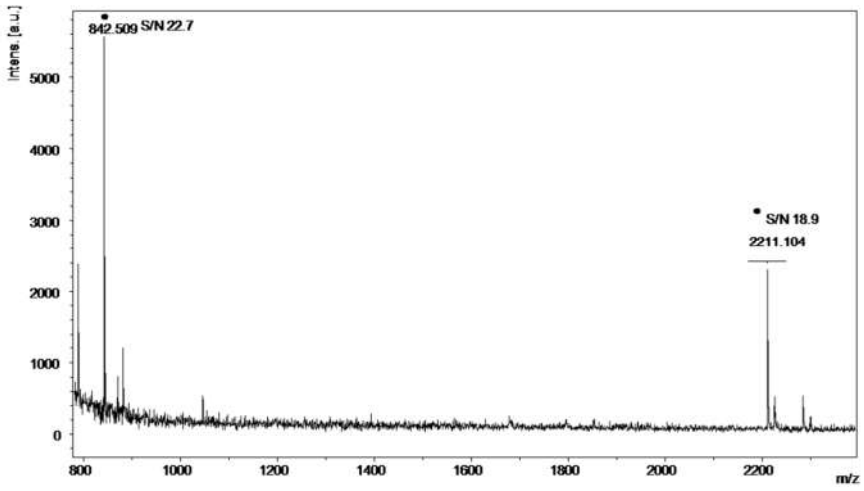

(**B**)

Figure 7. MALDI MS spectra of objects captured onto the SuccBB-activated AFM substrate surface. (**A**) C_{HSA} = 10^{-9} M; ●, trypsin autolysis peaks; ▲, HSA peptides; S/N, signal-to-noise ratio. (**B**) Control solution without protein: ●, trypsin autolysis peaks. The average square deviation is <150 ppm. S/N, signal-to-noise ratio.

4. Discussion

To study the protein capturing onto the surface of AFM substrates, activated with either succinimide crosslinker (DSP) or benzophenone (SuccBB) photoactivatable crosslinker, we have selected two model proteins with different physicochemical properties: horseradish peroxidase (HRP) and human serum albumin (HSA).

Based on the AFM and MS data obtained herein, one can state that activation of amino mica surface with DSP crosslinker provides efficient immobilization of only HRP enzyme protein—as opposed to the case with HSA, whose immobilization onto the DSP-activated surface has not been observed. That is, no objects, that could be attributed to HSA molecules, were observed on the substrate surface.

At the same time, in the case with SuccBB photocrosslinker, the immobilization of both HRP (in the form of extended aggregate structures) and HSA (in the form of layer fragments) can be considered to be efficient.

Quite low efficiency of immobilization of HSA onto the substrate bearing succinimide active groups can be explained by electrostatic effects occurring upon the interaction of HSA molecules with this surface. It is known that the net charge of a protein molecule depends on the pH of the medium, and is equal to zero at a pH corresponding to the protein's isoelectric point (*pI*). Accordingly, at pH < *pI* the protein molecules bear positive net charge, while at pH > *pI* their net charge is negative. Since pH of deionized water is slightly acidic (~5.8 [70]), in the absence of buffer salts in aqueous solution, HSA molecules bear negative net charge. Furthermore, according to the studies reported by Carré et al. [71] and Mori et al. [72], insignificant negative charge is present on the mica surface in the centers free from succinimide groups owing to the presence of SiO^- groups. Considering the possible influence of amino silane layer on the substrate surface, it is to be emphasized that the zeta potential of quartz surface (which also represents a silicate, similar to mica) is negative at pH>3 even in the presence of amino silane layer on it [62]. Moreover, as was noted in the introduction, the desired reaction of aminolysis of the captured protein is accompanied by the concurrent side reaction of hydrolysis of succinimide active groups. The latter process becomes dominant when protein concentration is low and pH is near the physiological one. In this way, a negative charge is also formed on the substrate surface owing to the hydrolysis of succinimide groups on it [73]. Accordingly, the resulting electrostatic repulsion between the negatively charged substrate surface and negatively charged HSA molecules can hinder their approach to this surface, resulting in the absence of immobilized HSA on it. It should be emphasized that the observed absence of immobilized HSA on the DSP-activated amino mica surface is in agreement with the previously obtained data on the adsorption of HSA onto amino silane surface at various pH studied by optical biosensor method [15]. In [15], only a very weak adsorption of HSA onto amino silane surface was observed at pH 6.0 and 7.4, while the concentration of HSA was 10^{-8} M, which is an order of magnitude higher than that used in the present study.

This limiting role of electrostatic interaction between the substrate surface and the protein to be immobilized also explains high efficiency of HRP immobilization in the case of DSP-activated surface. Since the *pI* of C-isoform of HRP is high (*pI* > 9 [59]), HRP molecules in solution are charged positively, and are thus readily captured onto the negatively charged substrate surface.

High immobilization efficiency of HSA upon the use of SuccBB photocrosslinker is primarily associated with the mechanism of the reaction between the protein and the crosslinker itself. The excitation of the photoactive group of benzophenone is performed at a wavelength of 350 to 370 nm. Upon irradiation, benzophenone generates a triplet ketyl radical, which mainly reacts with carbon-hydrogen (C–H) bonds in the protein, which are inactive when other crosslinkers are employed [74]. Thus, the reaction with SuccBB does not require the presence of certain functional groups in the protein, as was the case with amine groups upon the reaction with DSP. In this way, this distinctive feature of benzophenone-type crosslinkers allows immobilization of highly glycosylated proteins (and HRP is just the case [56–58]) and carbohydrates [75,76], when immobilization via primary amine groups can be difficult or is impossible. This favourable circumstance significantly increases the number of binding centers of the biomolecule with the active groups of the substrate surface. Of

course, since such non-selective binding may affect the biological functionality of the immobilized proteins, it should be monitored after the immobilization.

Moreover, the SuccBB-activated surface retains its binding properties for a long time owing to the absence of degradation of active groups during a long-term storage. The undoubted advantage is the reversibility of SuccBB photoactivation [74]. This allows for the multiple excitation with a long-wave UV light, what can be used for long-continued incubation. The latter is in demand for protein capturing from low-concentration solutions. Again, one more advantage of SuccBB photocrosslinker is that the required wavelength of the excitation UV light (350 to 370 nm) allows one to avoid damage to the protein structure [47,50].

The results obtained herein can be useful in the development of novel highly sensitive diagnostic platforms employing immobilized proteins. The obtained data can also be of interest for other research areas in medicine and biotechnology employing immobilized biomolecules.

5. Conclusions

Herein, the immobilization of two different proteins (HRP and HSA) onto the APTES-modified muscovite mica surface with succinimide and benzophenone crosslinkers (DSP and SuccBB) has been studied by AFM.

By using a combination of AFM with mass spectrometry analysis, both crosslinkers have been shown to be efficient for immobilization of HRP. In the case with HSA, only SuccBB photocrosslinker exhibited sufficient capturing efficiency. Inefficient immobilization of HSA upon using DSP can be explained by electrostatic repulsion effects, which hinder the approach of HSA molecules to the substrate surface.

Future studies will be aimed at determination of the sensitivity of photochemical protein fishing using the SuccBB crosslinker for detection of proteins at ultra-low concentrations.

The results obtained herein can find their application in commonly employed bioanalytical systems and in the development of novel highly sensitive chip-based diagnostic platforms employing immobilized proteins. The obtained data can also be of interest for other research areas in medicine and biotechnology employing immobilized biomolecules.

Author Contributions: Conceptualization, Yu.D.I. and T.O.P.; methodology, T.O.P.; software, V.S.Z.; validation, A.L.K.; formal analysis, A.A.V. and I.A.I.; investigation, A.A.V., A.L.K., I.A.I., V.S.Z. and T.O.P.; resources, Yu.D.I.; data curation, A.A.V. and I.A.I.; writing—original draft preparation, I.D.S. and T.O.P.; writing—review and editing, Yu.D.I.; visualization, A.A.V., I.D.S. and T.O.P.; supervision, Yu.D.I.; project administration, Yu.D.I.; funding acquisition, Yu.D.I. All authors have read and agreed to the published version of the manuscript.

Funding: The study was performed in the framework of the Program for Basic Research of State Academies of Sciences for 2013-2020.

Conflicts of Interest: The authors declare no conflict of interest.

References

1. Kasemo, B. Biological surface science. *Surf. Sci.* **2002**, *500*, 656–677, doi:10.1016/S1359-0286(98)80006-5.
2. Bilek, M.M.M. Biofunctionalization of surfaces by energetic ion implantation: Review of progress on applications in implantable biomedical devicesand antibody microarrays. *Appl. Surf. Sci.* **2014**, *310*, 3–10, doi:10.1016/j.apsusc.2014.03.0.
3. Pleshakova, T.O.; Kaysheva, A.L.; Shumov, I.D.; Ziborov, V.S.; Bayzyanova, J.M.; Konev, V.A.; Uchaikin, V.F.; Archakov, A.I.; Ivanov, Y.D. Detection of hepatitis C virus core protein in serum using aptamer-functionalized AFM chips. *Micromachines* **2019**, *10*, 129, doi:10.3390/mi10020129.
4. Tikhonov, A.A.; Savvateeva, E.N.; Chernichenko, M.A.; Maslennikov, V.V.; Sidorov, D.V.; Rubina, A.Y.; Kushlinskii, N.E. Analysis of Anti-Glycan IgG and IgM antibodies in colorectal cancer. *Bull. Exp. Biol. Med.* **2019**, *166*, 489–493, doi:10.1007/s10517-019-04379-2.
5. Jurczak, P.; Witkowska, J.; Rodziewicz-Motowidło, S.; Lach, S. Proteins, peptides and peptidomimetics as active agents in implant surface functionalization. *Adv. Coll. Interface Sci.* **2020**, *276*, 102083, doi:10.1016/j.cis.2019.102083.

6. Bayramoglu, G.; Arıca, M.Y. Enzymatic removal of phenol and p-chlorophenol in enzyme reactor: Horseradish peroxidase immobilized on magnetic beads. *J. Hazard. Mater.* **2008**, *156*, 148–155, doi:10.1016/j.jhazmat.2007.12.008.
7. Karami, F.; Ghorbani, M.; Alireza Sadeghi Mahoonak, A.S.; Khodarahmi, R. Fast, inexpensive purification of β-glucosidase from Aspergillus niger and improved catalytic/physicochemical properties upon the enzyme immobilization: Possible broad prospects for industrial applications. *LWT Food Sci. Technol.* **2020**, *118*, 108770, doi:10.1016/j.lwt.2019.108770.
8. Mohammadi, M.; Mokarrama, R.R.; Ghorbani, M.; Hamishehkar, H. Inulinase immobilized gold-magnetic nanoparticles as a magnetically recyclable biocatalyst for facial and efficient inulin biotransformation to high fructose syrup. *Int. J. Biol. Macromol.* **2019**, *123*, 846–855, doi:10.1016/j.ijbiomac.2018.11.160.
9. Furuya, T.; Kuroiwa, M.; Kino, K. Biotechnological production of vanillin using immobilized enzymes. *J. Biotechnol.* **2017**, *243*, 25–28, doi:10.1016/j.jbiotec.2016.12.021.
10. Wang, J.; Lia, K.; Hea, Y.; Wang, Y.; Han, X.; Yan, Y. Enhanced performance of lipase immobilized onto Co^{2+}-chelated magnetic nanoparticles and its application in biodiesel production. *Fuel* **2019**, *255*, 115794, doi:10.1016/j.fuel.2019.115794.
11. Meyers, S.R.; Khoo, X.; Huang, X.; Walsh, E.B.; Grinstaff, M.W.; Kenan, D.J. The development of peptide-based interfacial biomaterials for generating biological functionality on the surface of bioinert materials. *Biomaterials* **2009**, *30*, 277–286, doi:10.1016/j.biomaterials.2008.08.042.
12. Cho, S.-H.; Shim, J.; Yun, S.-H.; Moon, S.-H. Enzyme-catalyzed conversion of phenol by using immobilized horseradish peroxidase (HRP) in a membraneless electrochemical reactor. *Appl. Catal. A Gen.* **2008**, *337*, 66–72, doi:10.1016/j.apcata.2007.11.038.
13. Basso, A.; Serban, S. Industrial applications of immobilized enzymes—A review. *Mol. Catal.* **2019**, *479*, 110607, doi:10.1016/j.mcat.2019.110607.
14. Archakov, A.I.; Ivanov, Y.D.; Lisitsa, A.V.; Zgoda, V.G. Biospecific irreversible fishing coupled with atomic force microscopy for detection of extremely low-abundant proteins. *Proteomics* **2009**, *9*, 1326–1343, doi:10.1002/pmic.200800598.
15. Ivanov, Y.D.; Pleshakova, T.O.; Kozlov, A.F.; Malsagova, K.A.; Krohin, N.V.; Shumyantseva, V.V.; Shumov, I.D.; Popov, V.P.; Naumova, O.V.; Fomin, B.I.; et al. SOI nanowire for the high-sensitive detection of HBsAg and α-fetoprotein. *Lab Chip* **2012**, *12*, 5104–5111, doi:10.1039/c2lc40555e.
16. Ivanov, Y.D.; Kaysheva, A.L.; Frantsuzov, P.A.; Pleshakova, T.O.; Krohin, N.V.; Izotov, A.A.; Shumov, I.D.; Uchaikin, V.F.; Konev, V.A.; Ziborov, V.S.; et al. Detection of hepatitis C virus core protein in serum by atomic force microscopy combined with mass spectrometry. *Int. J. Nanomed.* **2015**, *10*, 1597–1608.
17. Truong, P.L.; Kim, B.W.; Sim, S.J. Rational aspect ratio and suitable antibody coverage of gold nanorod for ultra-sensitive detection of a cancer biomarker. *Lab Chip* **2012**, *12*, 1102–1109, doi:10.1039/C2LC20588B.
18. Ivanov, Y.D.; Bukharina, N.S.; Pleshakova, T.O.; Frantsuzov, P.A.; Andreeva, E.Y.; Kaysheva, A.L.; Zgoda, V.G.; Izotov, A.A.; Pavlova, T.I.; Ziborov, V.S.; et al. Atomic force microscopy fishing and mass spectrometry identification of gp120 on immobilized aptamers. *Int. J. Nanomed.* **2014**, *9*, 4659–4670.
19. Ivanov, A.S.; Medvedev, A.; Ershov, P.; Molnar, A.; Mezentsev, Y.; Yablokov, E.; Kaluzhsky, L.; Gnedenko, O.; Buneeva, O.; Haidukevich, I.; et al. Protein interactomics based on direct molecular fishing on paramagnetic particles: Practical realization and further SPR validation. *Proteomics* **2014**, *14*, 2261–2274, doi:10.1002/pmic.201400117.
20. Pleshakova, T.O.; Shumov, I.D.; Ivanov, Y.D.; Malsagova, K.A.; Kaysheva, A.L.; Archakov, A.I. AFM-based technologies as the way towards the reverse Avogadro number. *Biochem. Suppl. Ser. B Biomed. Chem.* **2015**, *9*, 244–257, doi:10.1134/S1990750815030063.
21. Rissin, D.M.; Kan, C.W.; Campbell, T.G.; Howes, S.C.; Fournier, D.R.; Song, L.; Piech, T.; Patel, P.P.; Chang, L.; Rivnak, A.J.; et al. Single-molecule enzyme-linked immunosorbent assay detects serum proteins at subfemtomolar concentrations. *Nat. Biotechnol.* **2010**, *28*, 595–599, doi:10.1038/nbt.1641.
22. Ivanov, Y.D.; Danichev, V.V.; Pleshakova, T.O.; Shumov, I.D.; Ziborov, V.S.; Krokhin, N.V.; Zagumenniy, M.N.; Ustinov, V.S.; Smirnov, L.P.; Archakov, A.I. Irreversible chemical AFM-based fishing for the detection of low-copied proteins. *Biochem. Suppl. Ser. B Biomed. Chem.* **2013**, *7*, 46–61, doi:10.1134/S1990750813010071.
23. Pleshakova, T.O.; Kaysheva, A.L.; Bayzyanova, J.M.; Anashkina, A.S.; Uchaikin, V.F.; Ziborov, V.S.; Konev, V.A.; Archakov, A.I.; Ivanov, Y.D. The detection of hepatitis c virus core antigen using AFM chips with immobolized aptamers. *J. Virol. Methods* **2018**, *251*, 99–105, doi:10.1016/j.jviromet.2017.10.015.

24. Braga, P.C.; Ricci, D. Atomic Force Microscopy. Biology: Biomedical Methods and Applications. In *Methods in Molecular Biology*; Humana Press: Totowa, NJ, USA, 2003; Volume 242, p. 382.
25. Crampton, N.; Bonass, W.A.; Kirkham, J.; Thomson, N.H. Formation of aminosilane-functionalized mica for atomic force microscopy imaging of DNA. *Langmuir* **2005**, *21*, 7884–7891, doi:10.1021/la050972q.
26. El Kirat, K.; Burton, I.; Dupres, V.; Dufrene, Y.F. Sample preparation procedures for biological atomic force microscopy. *J. Microsc.* **2005**, *218*, 199–207.
27. Shinohara, K.; Makida, Y. Direct observation of dynamic interaction between a functional group in a single SBR chain and an inorganic matter surface. *Sci. Rep.* **2018**, *8*, 13982, doi:10.1038/s41598-018-32382-6.
28. Kolb, D.; Kolb, K.E. The chemistry of glass. *J. Chem. Educ.* **1979**, *56*, 604–608, doi:10.1021/ed056p604.
29. Limanskaya, L.A.; Limanskii, A.P. Compaction of single supercoiled DNA molecules adsorbed onto amino mica. *Russ. J. Bioorganic Chem.* **2006**, *32*, 444–459, doi:10.1134/S1068162006050074.
30. Lyubchenko, Y.L.; Gall, A.A.; Shlyakhtenko, L.S.; Harrington, R.E.; Jacobs, B.L.; Oden, P.I.; Lindsay, S.M. Atomic force microscopy imaging of double stranded DNA and RNA. *J. Biomol. Struct. Dyn.* **1992**, *10*, 589–606, doi:10.1080/07391102.1992.10508670.
31. Lyubchenko, Y.L.; Shlyakhtenko, L.S.; Harrington, R.E.; Oden, P.I.; SMLindsay, S.M. Atomic force microscopy of long DNA: Imaging in air and under water. *Proc. Natl. Acad. Sci. USA* **1993**, *90*, 2137–2140, doi:10.1073/pnas.90.6.2137.
32. Shlyakhtenko, L.S.; Gall, A.A.; Weimer, J.J.; Hawn, D.D.; Lyubchenko, Y.L. Atomic force microscopy imaging of dna covalently immobilized on a functionalized mica substrate. *Biophys. J.* **1999**, *77*, 568–576, doi:10.1016/S0006-3495(99)76913-4.
33. Shlyakhtenko, L.S.; Gall, A.A.; Lyubchenko, Y.L. Mica functionalization for imaging of DNA and protein-DNA complexes with atomic force microscopy. *Methods Mol. Biol.* **2013**, *931*, doi:10.1007/978-1-62703-056-4_14.
34. Wang, H.; Bash, R.; Yodh, J.G.; Hager, G.L.; Lohr, D.; Lindsay, S.M. Glutaraldehyde modified mica: A new surface for atomic force microscopy of chromatin. *Biophys. J.* **2002**, *83*, 3619–3625, doi:10.1016/S0006-3495(02)75362-9.
35. Ierardi, V.; Ferrera, F.; Millo, E.; Damonte, G.; Filaci, G.; Valbusa, U. Bioactive surfaces for antibody-antigen complex detection by Atomic Force Microscopy. *J. Phys. Conf. Ser.* **2013**, *439*, 012001, doi:10.1088/1742-6596/439/1/012001.
36. Mattson, G.; Conklin, E.; Desai, S.; Nielander, G.; Savage, M.D.; Morgensen, S. A practical approach to crosslinking. *Mol. Biol. Rep.* **1993**, *17*, 167–183, doi:10.1007/BF00986726.
37. Stanković, V.; Đurđić, S.; Ognjanović, M.; Antić, B.; Kalcher, K.; Mutić, J.; Stanković, D.M. Anti-human albumin monoclonal antibody immobilized on EDC-NHS functionalized carboxylic graphene/AuNPs composite as promising electrochemical HSA immunosensor. *J. Electroanal. Chem.* **2020**, *860*, 113928, doi:10.1016/j.jelechem.2020.113928.
38. Sam, S.; Touahir, L.; Andresa, J.S.; Allongue, P.; Chazalviel, J.-N.; Gouget-Laemmel, A.C.; de Villeneuve, C.H.; Moraillon, A.; Ozanam, F.; Gobouze, N.; et al. Semiquantitative Study of the EDC/NHS Activation of Acid Terminal Groups at Modified Porous Silicon Surfaces. *Langmuir* **2010**, *26*, 809–814, doi:10.1021/la902220a.
39. Shikha, S.; Thakur, K.G.; Bhattacharyya, M.S. Facile fabrication of lipase to amine functionalized gold nanoparticles to enhance stability andactivity. *RSC Adv.* **2017**, *7*, 42845–42855, doi:10.1039/c7ra06075k.
40. Migneault, I.; Dartiguenave, C.; Bertrand, M.J.; Waldron, K.C. Glutaraldehyde: Behavior in aqueous solution, reaction with proteins, and application to enzyme crosslinking. *BioTechniques* **2004**, *37*, 790–802.
41. Carvalho, F.; Paradiso, P.; Saramago, B.; Ferraria, A.M.; do Rego, A.M.B.; Fernandes, P. An integrated approach for the detailed characterization of an immobilized enzyme. *J. Mol. Catal. B Enzym.* **2016**, *125*, 64–74, doi:10.1016/j.molcatb.2016.01.001.
42. Hermanson, G.T. *Bioconjugate Techniques*, 3rd ed.; Academic Press: Cambridge, MA, USA; Elsevier: Amsterdam, The Netherlands, 2013; p. 1200.
43. Orrego, A.H.; Romero-Fernández, M.; del Carmen Millán-Linares, M.; del Mar Yust, M.; Guisán, J.M.; Rocha-Martin, J. Stabilization of Enzymes by Multipoint Covalent Attachment on Aldehyde-Supports: 2-Picoline Borane as an Alternative Reducing Agent. *Catalysts* **2018**, *8*, 333, doi:10.3390/catal8080333.
44. Rodrigues, D.S.; Mendes, A.A.; Adriano, W.S.; Goncalves, L.R.B.; Giordano, R.L.C. Multipoint covalent immobilization of microbial lipase on chitosan and agarose activated by different methods. *J. Mol. Catal. B Enzym.* **2008**, *51*, 100–109, doi:10.1016/j.molcatb.2007.11.016.

45. Karrasch, S.; Dolder, M.; Schabert, F.; Ramsden, J.; Engel, A. Covalent binding of biological samples to solid supports for scanning probe microscopy in buffer solution. *Biophys. J.* **1993**, *65*, 2437–2446, doi:10.1016/S0006-3495(93)81327-4.
46. Voskresenska, V.; Wilson, R.M.; Panov, M.; Tarnovsky, A.N.; Krause, J.A.; Vyas, S.; Winter, A.H.; Hadad, C.M. Photoaffinity labeling via nitrenium ion chemistry: Protonation of the nitrene derived from 4-amino-3-nitrophenyl azide to afford reactive nitrenium ion pairs. *J. Am. Chem. Soc.* **2009**, *131*, 11535–11547, doi:10.1021/ja902224m.
47. Surmanjit, J.; Chung, S.J. Recent advances in target characterization and identification by photoaffinity probes. *Molecules* **2013**, *18*, 10425–10451, doi:10.3390/molecules180910425.
48. Dorman, G.; Prestwich, G.D. Benzophenone photophores in biochemistry. *Perspect. Biochem.* **1994**, *33*, 5661–5673, doi:10.1021/bi00185a001.
49. Kim, D.; Herr, A.E. Protein immobilization techniques for microfluidic assays. *Biomicrofluidics* **2013**, *7*, 041501, doi:10.1063/1.4816934.
50. Chin, J.W.; Martin, A.B.; King, D.S.; Wang, L.; Schultz, P.G. Addition of a photocrosslinking amino acid to the genetic code of Escherichia coli. *Proc. Natl. Acad. Sci. USA* **2002**, *99*, 11020–11024, doi:10.1073/pnas.172226299.
51. Williams, N.; Ackerman, S.H.; Coleman, P.S. Benzophenone-ATP: A photoaffinity label for the active site of ATPases. In *Methods in Enzymology*; Academic Press: Cambridge, MA, USA, 1986; Volume 126, pp. 667–682.
52. Prestwich, G.D.; Dorman, G.; Elliott, J.T.; Marecak, D.M.; Chaudhary, A. Benzophenone photoprobes for phosphoinositides, peptides and drugs. *Photochem. Photobiol.* **1997**, *65*, 222–234, doi:10.1111/j.1751-1097.1997.tb08548.x.
53. Tsai, H.; Doong, R.; Lin, C. A strategy for multi-protein-immobilization using N-succinimidyl 4-Benzoylbenzoic acid as the photolabile ligand. *Anal. Sci./Suppl.* **2001**, *17icas*, i269–i272, doi: 10.14891/analscisp.17icas.0.i269.0.
54. Wu, X.; Tang Qi Liu, C.; Li, Q.; Guo, Y.; Yang, Y.; Lv, X.; Geng, L.; Deng, Y. Protein photoimmobilizations on the surface of quartz glass simply mediated by benzophenone. *Appl. Surf. Sci.* **2011**, *257*, 7415–7421, doi:10.1016/j.apsusc.2011.02.106.
55. Davies, P.F.; Rennke, H.G.; Cotran, R.S. Influence of molecular charge upon the endocytosis and intracellular fate of peroxidase activity in cultured arterial endothelium. *J. Cell Sci.* **1981**, *49*, 69–86.
56. Welinder, K.G. Amino acid sequence studies of horseradish peroxidase. amino and carboxyl termini, cyanogen bromide and tryptic fragments, the complete sequence, and some structural characteristics of horseradish peroxidase C. *Eur. J. Biochem.* **1979**, *96*, 483–502, doi:10.1111/j.1432-1033.1979.tb13061.x.
57. Shannon, L.M.; Kay, E.; Lew, J.Y. Peroxidase isozymes from horseradish roots I. Isolation and physical properties. *J. Biol. Chem.* **1966**, *241*, 2166–2172.
58. Tams, J.W.; Welinder, K.G. Mild chemical deglycosylation of horseradish peroxidase yields a fully active, homogeneous enzyme. *Anal. Biochem.* **1995**, *228*, 48–55, doi:10.1006/abio.1995.1313.
59. Aibara, S.; Yamashua, H.; Mori, E.; Kato, M.; Morita, Y. Isolation and characterization of five neutral isoenzymes of horseradish peroxidase. *J. Biochem.* **1982**, *92*, 531–539, doi:10.1093/oxfordjournals.jbchem.a133961.
60. Artimo, P.; Jonnalagedda, M.; Arnold, K.; Baratin, D.; Csardi, G.; de Castro, E.; Duvaud, S.; Flegel, V.; Fortier, A.; Gasteiger, E.; et al. ExPASy: SIB bioinformatics resource portal. *Nucl. Acids Res.* **2012**, *40*, W597–W603, doi:10.1093/nar/gks400.
61. Carter, D.C.; Ho, J.X. Structure of serum albumin. *Adv. Protein Chem.* **1994**, *45*, 153–203.
62. Yamada, K.; Yoshii, S.; Kumagai, S.; Fujiwara, I.; Nishio, K.; Okuda, M.; Matsukawa, N.; Yamashita, I. High-density and highly surface selective adsorption of protein–nanoparticle complexes by controlling electrostatic interaction. *Jpn. J. Appl. Phys.* **2006**, *45 part 1 (5A)*, 4259–4264, doi:10.1143/JJAP.45.4259.
63. Huff, J.; Lynch, M.P.; Nettikadan, S.; Johnson, J.C.; Vengasandra, S.; Henderson, E. Label-free protein and pathogen detection using the atomic force microscope. *J. Biomol. Screen.* **2004**, *9*, 491–497, doi:10.1177/1087057104268803.
64. Kaysheva, A.L.; Pleshakova, T.O.; Stepanov, A.A.; Ziborov, V.S.; Saravanabhavan, S.S.; Natesan, B.; Archakov, A.I.; Ivanov, Y.D. Immuno-MALDI MS dataset for improved detection of HCVcoreAg in sera. *Data Brief.* **2019**, *25*, 104240, doi:10.1016/j.dib.2019.104240.
65. Ivanov, Y.D.; Pleshakova, T.; Malsagova, K.; Kozlov, A.; Kaysheva, A.; Kopylov, A.; Izotov, A.; Andreeva, E.; Kanashenko, S.; Usanov, S.; et al. Highly sensitive protein detection by combination of atomic force

microscopy fishing with charge generation and mass spectrometry analysis. *FEBS J.* **2014**, *281*, 4705–4717, doi:10.1111/febs.13011.
66. Ivanov, Y.D.; Pleshakova, T.O.; Krohin, N.V.; Kaysheva, A.L.; Usanov, S.A.; Archakov, A.I. Registration of the protein with compact disk. *Biosens. Bioelectron.* **2013**, *43*, 384–390, doi:10.1016/j.bios.2012.12.039.
67. Ignatenko, O.V.; Sjölander, A.; Hushpulian, D.M.; Kazakov, S.V.; Ouporov, I.V.; Chubar, T.A.; Poloznikov, A.A.; Ruzgas, T.; Tishkov, V.I.; Gorton, L.; et al. Electrochemistry of chemically trapped dimeric and monomeric recombinant horseradish peroxidase. *Adv. Biosens. Bioelectron.* **2013**, *2*, 25–34.
68. UniProt KB. Available online: http://www.uniprot.org/ (accessed on 19 May 2020).
69. Kowalczyk, D.; Marsault, J.-P.; Slomkowski, S. Atomic force microscopy of human serum albumin (HSA) on poly(styrene/acrolein) microspheres. *Colloid Polym. Sci.* **1996**, *274*, 513–519, doi:10.1007/BF00655225.
70. Chen, S.L.; Chen, C.T.; Kao, C.H. Acidification of deionized water by roots of intact rice seedings. *Plant. Cell Physiol.* **1990**, *31*, 569–573.
71. Carré, A.; Lacarrière, V.; Birch, W. Molecular interactions between DNA and an aminated glass substrate. *J. Coll. Interface Sci.* **2003**, *260*, 49–55.
72. Mori, O.; Imae, T. AFM investigation of the adsorption process of bovine serum albumin on mica. *Coll. Surf. B: Biointerfaces* **1997**, *9*, 31–36.
73. Lim, C.Y.; Owens, N.A.; Wampler, R.D.; Ying, Y.; Granger, J.H.; Porter, M.D.; Takahashi, M.; Shimazu, K. Succinimidyl ester surface chemistry: Implications of the competition between aminolysis and hydrolysis on covalent protein immobilization. *Langmuir* **2014**, *30*, 12868–12878.
74. Preston, G.W.; Wilson, A.J. Photo-induced covalent cross-linking for the analysis of biomolecular interactions. *Chem. Soc. Rev.* **2013**, *42*, 3289–3301, doi:10.1039/C3CS35459H.
75. Toh C.R.; Fraterman T.A.; Walker D.A.; Bailey R.C. A direct biophotolithographic method for generating substrates with multiple overlapping biomolecular patterns and gradients. *Langmuir* **2009**, *25*, 8894–8898. doi:10.1021/la9019537.
76. Turgeon A.J.; Harley B.A.; Bailey R.C. Benzophenone-based photochemical micropatterning of biomolecules to create model substrates and instructive biomaterials. In *Methods in Cell Biology*, Elsevier: Amsterdam, The Netherlands, 2014; Volume 121, pp. 231–242.